

Topological Quantum Optics in Two-Dimensional Atomic Arrays

J. Perczel,^{1,2} J. Borregaard,² D. Chang,³ H. Pichler,^{2,4} S. F. Yelin,^{2,5} P. Zoller,^{6,7} and M. D. Lukin²

¹*Physics Department, Massachusetts Institute of Technology, Cambridge, MA 02139, USA*

²*Physics Department, Harvard University, Cambridge, MA 02138, USA*

³*ICFO - Institut de Ciències Fotoniques, The Barcelona Institute of Science and Technology, 08860 Castelldefels, Barcelona, Spain*

⁴*ITAMP, Harvard-Smithsonian Center for Astrophysics, Cambridge, MA 02138, USA*

⁵*Department of Physics, University of Connecticut, Storrs, Connecticut 06269, USA*

⁶*Institute for Theoretical Physics, University of Innsbruck, A-6020 Innsbruck, Austria*

⁷*Institute for Quantum Optics and Quantum Information of the Austrian Academy of Sciences, A-6020 Innsbruck, Austria*

(Dated: March 16, 2017)

We demonstrate that two-dimensional atomic arrays with subwavelength spacing can be used to create topologically protected quantum optical systems where the photon propagation is robust against large imperfections while losses associated with free space emission are strongly suppressed. Breaking time-reversal symmetry with a magnetic field results in gapped photonic bands with non-trivial Chern numbers. Such a system displays topologically protected bound states and unidirectional emission by individual atoms into long-lived edge states. Possible experimental realizations and applications are discussed.

PACS numbers: 42.50.Ex

Charged particles in two-dimensional systems exhibit exotic macroscopic behavior in the presence of magnetic fields and interactions. These include the integer [1], fractional [2] and spin [3] quantum Hall effects. In particular, such systems support topologically protected edge states [4, 5] that are robust against defects and disorder. Such topological protection has been identified as a possible route for fault-tolerant quantum information systems [6, 7]. There is a significant interest in realizing topologically protected photonic systems. Photonic analogues of quantum Hall behavior have been studied in gyromagnetic photonic crystals [8–12], helical waveguides [13], two-dimensional lattices of optical resonators [14–16] and in polaritons coupled to optical cavities [17]. An outstanding challenge is to realize optical systems which are robust not only to some specific backscattering processes but to *all* loss processes, including scattering into unconfined modes and spontaneous emission. Another challenge is to extend these effects into a quantum domain with strong interactions between individual photons.

In this Letter, we introduce and analyze a novel platform for engineering topological states in the optical domain. It is based on atomic quantum optical systems, where parameters can be tuned over a wide range, coherences are long-lived and time-reversal symmetry can be broken by applying magnetic fields. Specifically, we focus on optical excitations in a two-dimensional honeycomb array of closely spaced atomic emitters. We show that such systems maintain topologically protected confined optical modes that are immune to large imperfections as well as to most common loss processes such as scattering into free-space modes [18, 19]. Such modes can be used to control individual atom emission, and to create quantum nonlinearity at a single photon level.

The key idea is illustrated in Fig. 1(a). We envision an atomic array with interatomic spacing p and quantization axis \hat{z} perpendicular to the plane of the atoms. Each atom has a V-type level structure with transitions from the ground state to the excited states $|\sigma_+\rangle$ and $|\sigma_-\rangle$, excited by the corresponding polarization components of light [20]. The hybridized atomic and photonic states in such arrays result in confined Bloch modes with large characteristic quasi-momenta that for dense atomic arrays significantly exceed the momentum of free-space photons. These confined modes are outside of the so-called “light cone” and are decoupled from free space resulting in long-lived, effectively sub-radiant states [18, 19]. Atomic Zeeman-shifts induced by a magnetic field, create a bandgap in the optical excitation spectrum, and the Bloch bands acquire non-trivial Chern numbers. As we show below, the resulting system displays all essential features associated with topological robustness and strongly suppressed conventional optical losses. Before proceeding, we note that polar molecules coupled via near-field interactions [21, 22] in 2D have been shown to give rise to chiral excitations. In contrast, the present analysis includes both near- and far-field effects as well as, scattering and spontaneous emission relevant for the optical domain. We also note that the emergence of Weyl excitations has been recently predicted [23] in 3D lattices of polar particles.

In the single atomic excitation limit, following the adiabatic elimination of the photonic modes, the dynamics of the system (no-jump evolution in the master equation [24]) can be described by the following non-Hermitian

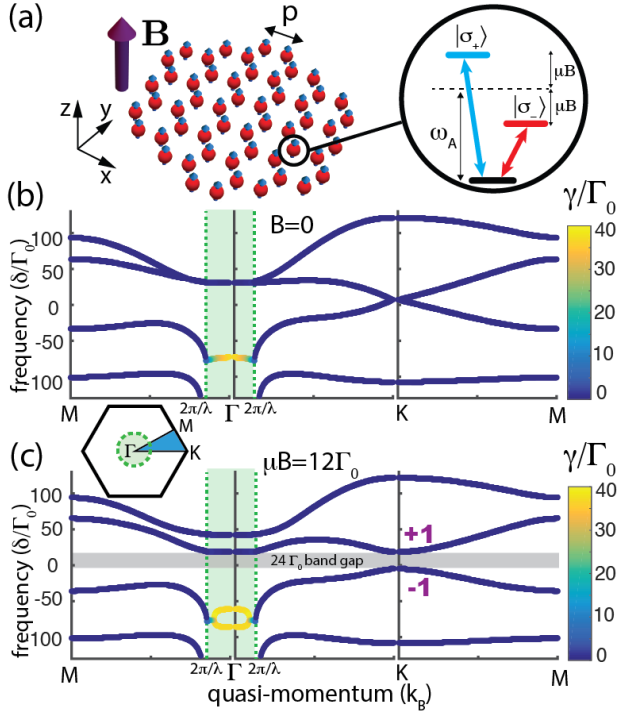


FIG. 1. (a) Honeycomb lattice of atomic emitters with interatomic spacing p . Each atom has a V-type level structure with transitions to the $|\sigma_+\rangle$ and $|\sigma_-\rangle$ states. B-field breaks the degeneracy through the Zeeman splitting. (b) Band structure of the lattice with $B = 0$. The edges of the free-space light cone are indicated by green dashed lines. Modes with quasi-momentum $k_B < \omega/c$ couple to free-space modes and are short lived (green shaded region). Decay rates of the modes are color-coded. Bands are degenerate at the symmetry points \mathbf{K} and $\mathbf{\Gamma}$. (c) Transverse magnetic field ($\mu B = 12\Gamma_0$) opens a gap (grey-shaded region) between topological bands with non-trivial Chern numbers. Relevant parameters are $\lambda = 790\text{nm}$, $\Gamma_0 = 6\text{MHz}$ and $p = 0.05\lambda$.

spin Hamiltonian [18, 25–28]

$$H = \hbar \sum_{i=1}^N \sum_{\alpha=\sigma_+, \sigma_-} \left(\omega_A + \text{sgn}(\alpha)\mu B - i\frac{\Gamma_0}{2} \right) |\alpha_i\rangle\langle\alpha_i| + \frac{3\pi\hbar\Gamma_0 c}{\omega_A} \sum_{i \neq j} \sum_{\alpha, \beta=\sigma_+, \sigma_-} G_{\alpha\beta}(\mathbf{r}_i - \mathbf{r}_j) |\alpha_i\rangle\langle\beta_j|, \quad (1)$$

where N is the number of atoms, $\omega_A = 2\pi c/\lambda$ is the atomic transition frequency with wavelength λ , μB is the Zeeman-shift of the atoms with magnetic moment μ in the presence of an out-of-plane magnetic field $\mathbf{B} = B\hat{z}$ with $\text{sgn}(\sigma_{\pm}) = \pm$. Here $\Gamma_0 = d^2\omega_A^3/(3\pi\epsilon_0\hbar c^3)$ is the radiative linewidth of an individual atom in free space, c is the speed of light, d is the transition dipole moment, $G_{\alpha\beta}(\mathbf{r})$ is the dyadic Green's function in free space describing the dipolar spin-spin interaction [29] and \mathbf{r}_i denotes the position vectors of the individual atoms. Note that the Hamiltonian in Eq. (1) assumes that the position of the atoms is fixed at the sites of the honeycomb lattice.

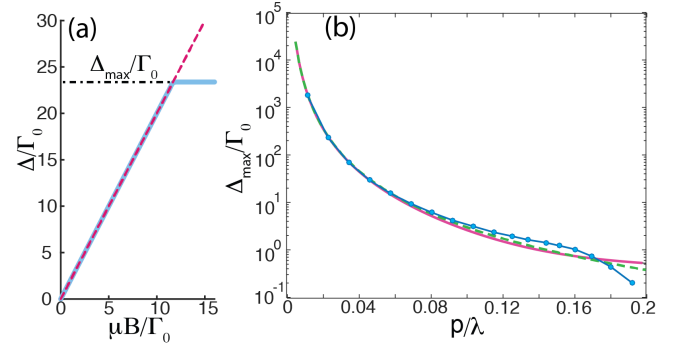


FIG. 2. (a) Size of the gap between topological bands (blue line) as a function of magnetic field for $p = \lambda/20$. (b) The maximum gap size Δ_{\max} (blue dotted line) as a function of the interatomic spacing p . The solid magenta line shows the dipolar interaction strength J between two atoms with parallel dipole moments. The dashed green line is a phenomenological $J \sim 1/r^3$ fit. Since for $p \ll \lambda$ the gap size Δ_{\max} is set by the dipolar interaction strength J , the gap scales as $1/p^3$ for deeply subwavelength lattices.

The effect of fluctuating atomic positions is discussed in Ref. [29].

For an infinite periodic honeycomb lattice, the single excitation eigenmodes of Eq. (1) are Bloch modes [30] given by

$$|\psi\rangle = \sum_n \sum_{q=1,2} e^{i\mathbf{k}_B \cdot \mathbf{R}_n} \left(c_{\sigma_+}^q |\sigma_{+,n}^q\rangle + c_{\sigma_-}^q |\sigma_{-,n}^q\rangle \right), \quad (2)$$

where the summation runs over all lattice vectors $\{\mathbf{R}_n\}$, $q = 1, 2$ labels the two atoms within the unit cell of the honeycomb lattice and \mathbf{k}_B is the Bloch wavevector. Fig. 1(b) shows the corresponding band structure in the absence of a magnetic field. The bands are plotted along the lines joining the high symmetry points \mathbf{M} , $\mathbf{\Gamma}$ and \mathbf{K} of the irreducible Brillouin zone (see inset of Fig. 1(c)). The complex part of the eigenvalues of the Hamiltonian in Eq. (1) corresponds to the decay rates γ of the Bloch modes, which are shown in Fig. 1 using a color code. Green dashed lines at $k_B = 2\pi/\lambda$ mark the edges of the light cone corresponding to free space modes with energies $\omega(k_B) = k_B c$ [19]. The light cone edges appear vertical in Fig. 1 since we are only looking at an energy range that is within a few hundred linewidths of ω_A and $\Gamma_0 \ll \omega_A$ at optical frequencies. The modes close to the center of the Brillouin zone ($\mathbf{\Gamma}$) have quasi-momenta k_B less than the maximum momentum of free space photons at the same energy ($k_B < \omega/c$). These modes couple strongly to free-space modes with matching energy and momentum and decay rapidly. In contrast, modes with quasi-momenta greater than the momentum of free space photons ($k_B > \omega/c$), are completely decoupled and do not decay into free space due to the momentum mismatch [19].

Fig. 1(b) also shows that in the absence of a magnetic

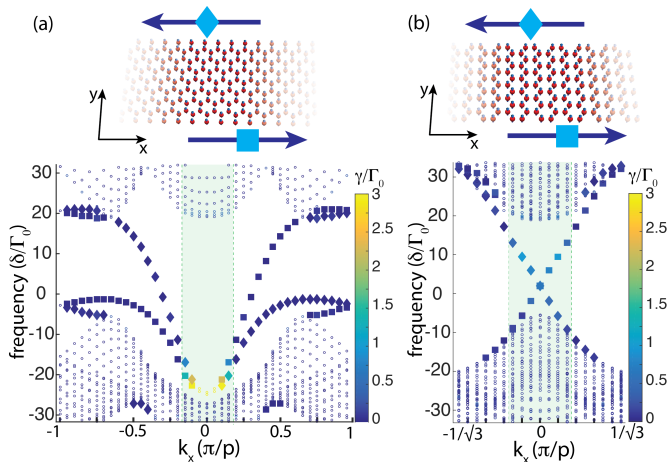


FIG. 3. Topological edge states on the (a) bearded and (b) armchair edges of periodic stripes of atoms. Each edge supports only one unidirectional mode. Modes propagating on the upper (lower) edges of the stripes are marked by diamonds (squares) in the band diagrams. Bulk modes are marked with dots. Decay rates of the modes are color-coded. Modes of the bearded (armchair) edges cross the gap with quasi-momentum $k_B > \omega/c$ ($k_B < \omega/c$) making them long (short) lived. Parameters are the same as in Fig. 1(c). The spectrum was obtained for the bearded (armchair) edges from an 80×42 (80×41) lattice of atoms with periodic boundary conditions along the longer dimension. States with more than 67% of their total amplitude on the top/bottom four atom rows are classified as edge states.

field, the photonic bands are degenerate at the high symmetry points Γ and \mathbf{K} of the Brillouin zone. A quadratic degeneracy is formed at the Γ point while a Dirac cone is formed at the \mathbf{K} point. These degeneracies originate from the degeneracy of the $|\sigma_+\rangle$ and $|\sigma_-\rangle$ states at zero magnetic field. Applying a magnetic field perpendicular to the plane of the lattice lifts this degeneracy and an energy gap forms across the Brillouin zone.

We explore the topological nature of these bands, by calculating the Chern numbers using the method described in Ref. [31]. The sum of the Chern numbers of the bands above and below the band gap is $+1$ and -1 respectively. This confirms that gapping out the Dirac cone leads to the exchange of one unit of Berry flux between the two middle bands. This is a key signature of topology [32].

Since the Zeeman splitting between the $|\sigma_+\rangle$ and $|\sigma_-\rangle$ states ($2\mu B$) is proportional to the magnetic field strength, the size of the gap between the top and bottom of the Dirac point at the \mathbf{K} point in the Brillouin zone scales linearly with the magnetic field (Fig. 2(a)). However, the size of the gap is eventually limited to a maximum value Δ_{\max} by the fact that the level repulsion between the two upper bands at the location of the quadratic degeneracy (Γ point in Brillouin zone) pushes some of the modes down into the gap. Fig. 2(b) shows

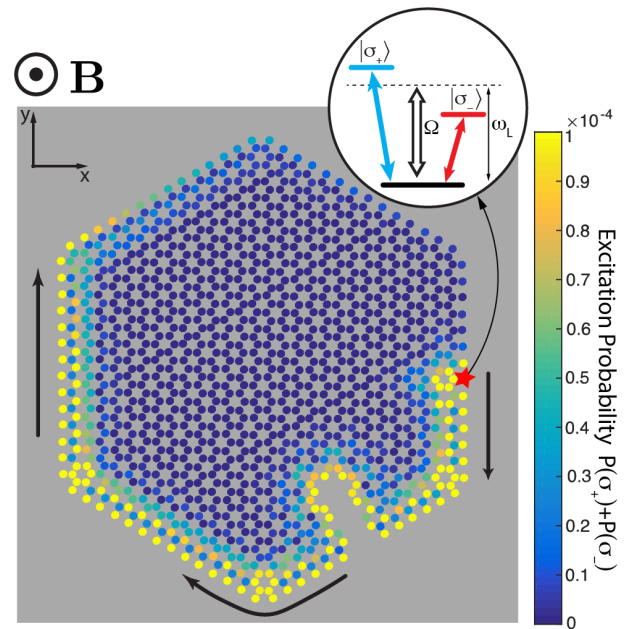


FIG. 4. Snapshot of the time evolution (at $t = 5.6\Gamma_0^{-1}$) of the system as an atom on the edge (red star) is driven by a laser (inset). The color code shows the excitation probability $|\langle\psi(t)|\sigma_+\rangle|^2 + |\langle\psi(t)|\sigma_-\rangle|^2$ at each atomic site. Approximately 95% of the excitation emitted by the atom is coupled into the forward direction and scattering into the bulk and backward edge modes is strongly suppressed. The excitation goes around the corners and routes around the large lattice defect. Relevant parameters are $N = 1243$, $\lambda = 790\text{nm}$, $\Gamma_0 = 6\text{MHz}$ and $p = 0.05\lambda$. The strength of the drive is $\Omega = 1/5\Gamma_0$ and the driving frequency is $\omega_L = \omega_A + 15\Gamma_0$. The driving laser is adiabatically switched on with a Gaussian profile $\Omega(t) = \Omega \exp(-[t - 1.5\Gamma_0^{-1}]^2/1.5\Gamma_0^{-1})$ for $t < 1.5\Gamma_0^{-1}$.

the maximum gap size as a function of the interatomic spacing p (blue dotted line). The strength of the dipolar coupling $J = 3\pi\Gamma_0 c/\omega_A G_{xx}(p)$ between two parallel dipoles at a distance p apart is also shown. The close agreement between the two curves shows that the maximum gap size is determined by the strength of the dipolar interaction between the atoms. For $r \ll \lambda$ the dipolar interaction scales as $J \sim 1/r^3$ (green dashed line). Therefore, the maximum gap size between the topological bands has the simple scaling $\Delta_{\max} \sim 1/p^3$ in a deeply subwavelength lattice.

Gaps between topological bands are typically associated with the presence of one-way reflection-free edge modes at the boundaries of a finite system. To explore the spectrum and dispersion of edge modes in the gap, we calculated the band structure for periodic stripes of atoms in a honeycomb lattice. Depending on the orientation of the lattice, the stripes may have bearded, armchair or zig-zag edges [32, 33]. Fig. 3 shows the edge geometries and the corresponding band structures of stripes with bearded and armchair edges. Zig-zag edges are discussed in Ref. [29]. Edge modes on the lower edge of the

stripe (marked with squares in Fig. 3) that traverse the band gap between the two bulk bands have positive group velocity carrying energy to the right. Edge modes of the upper edge (marked with diamonds in Fig. 3) have negative group velocity as they traverse the gap and carry energy to the left. Since the modes on each edge carry energy only in a single direction, energy transport by edge modes is unidirectional. This unidirectionality is a direct consequence of the broken time-reversal symmetry of the topological system. If the direction of the magnetic field is flipped, the direction of the energy flow on any given edge is also reversed. Edge modes on bearded boundaries have quasi-momenta $k_B > \omega/c$ while crossing the gap and therefore couple weakly to free-space modes making them long-lived. In contrast, modes on the armchair edges cross the gap with quasi-momenta $k_B < \omega/c$ and the relatively strong coupling to free-space modes makes them short-lived. Modes on zig-zag edges cross the light cone in the middle of the gap [29]. The lifetimes of edge modes are also influenced by the size of the lattice. Increasing the number of atoms N in a finite lattice decreases the losses arising from finite-size effects and increases the lifetimes of long-lived edge modes with quasi-momenta $k_B > \omega/c$ [29]. In contrast, changing the size of the lattice has little effect on the decay rate of short-lived edge modes with quasi-momenta $k_B < \omega/c$, whose loss via out-of-plane emission dominates.

Fig. 4 illustrates the unidirectional energy transport by topological edge states. The figure shows a honeycomb lattice of atoms with an overall hexagonal shape and a large defect on the edge. The geometry was chosen such that in the absence of any defects, all boundaries would be bearded edges supporting long-lived edge modes. An out-of-plane magnetic field \mathbf{B} induces a band gap of size Δ in the energy spectrum. An atom on the boundary is addressed by a laser at a frequency ω_L resonant with the edge modes in the topmost part of the band gap, where the bearded and zig-zag edge modes are long-lived and the armchair edge modes are close to the light cone boundaries. The laser drives the σ_+ and σ_- transitions of the atom off-resonantly with equal coupling strengths Ω , where $\Omega \ll \Delta$. The driving laser is adiabatically switched on to avoid exciting non-resonant modes and continuously excites the atom. Fig. 4 shows a snapshot of the excitation probability of each atom in the lattice. Approximately 95% of the excitation emitted by the driven atom is coupled into the edge modes carrying energy in the forward direction. Coupling into the backward direction or into the bulk modes is suppressed due to topology and the large band gap. Note that these results are qualitatively independent of the relative driving strength of the σ_- and σ_+ transitions. If only the σ_- or σ_+ transitions are driven, the efficiency of coupling into the unidirectional edge modes changes to 92% and 98% respectively. These results demonstrate that the unidirectionality arises from topology and not from

polarization selection as, for example, in Ref. [34]. Due to topological protection, the excitation routes around lattice corners with $\sim 94\%$ efficiency. In addition, the excitation also goes around defects of arbitrary shape and size by forming new edge modes at the boundaries of the defect as shown in Fig. 4, where $\sim 86\%$ of the excitation survives.

In general, the distance the photon propagates on any type of edge is set by the ratio of the group velocity and the intrinsic lifetime of the edge modes. The group velocity of the edge modes traversing the band gap is $v_g \approx \delta\omega/\delta k_B \sim \Delta/(\pi/p)$, where Δ is the size of the energy gap and p is the interatomic spacing. Thus the time it takes for the excitation to hop from one atom to the next scales as $\sim \Delta^{-1}$. Consequently, increasing the gap size leads to faster propagation of the photon along the lattice edges. Since the maximum gap size scales as $\Delta_{\max} \sim p^{-3}$ for small distances (Fig. 2), the maximum group velocity of the edge modes scales as $v_g \sim \Delta_{\max}/(\pi/p) \sim p^{-2}$. While bearded edges support long-lived modes, any departure from the ideal hexagonal shape of Fig. 4 creates a combination of armchair and zig-zag modes that couple more strongly to free-space modes and thus have limited lifetimes. To ensure that only a small fraction of the excitation is lost while the photon is routed around a defect, large group velocities and, therefore, large energy gaps are required. Thus lattices with small interatomic spacing are generally the most robust against disorder.

At energies inside the band gap there are no extended bulk modes. Therefore, when an atom in the bulk of the lattice is driven by a laser, whose frequency ω_L falls inside the gap, the atom cannot resonantly couple to any of the extended lattice modes. Instead, the atom weakly dresses the far-detuned modes. Consequently, the atom exchanges energy only with atoms in its immediate neighborhood and a spatially confined atom-photon bound state is formed [29]. This is analogous to the atom-photon bound states that are predicted to exist in photonic crystals with band gaps [35, 36]. Since the majority of the extended bulk modes above and below the band gap are long-lived, the bound state itself is sub-radiant with a decay rate of $\gamma/\Gamma_0 = 0.13 - 0.21$ depending on the polarization of the exciting laser [29].

These results demonstrate that subwavelength atomic lattices in the presence of a uniform magnetic field form topologically protected quantum optical systems, where emission to free space is strongly suppressed and photon propagation is robust against very large defects. Subwavelength trapping of atoms can be realized, for example, using Sr atoms as described in Refs. [23, 37], where the combination of long transition wavelengths ($\lambda_{\text{Sr}} = 2.6\mu\text{m}$) and a blue-detuned trapping laser with $\lambda_{\text{laser}} = 412.8\text{nm}$ would give rise to $p = 2\lambda_{\text{laser}}/(3\sqrt{3}) = \lambda_{\text{Sr}}/16.3$ in an optical honeycomb lattice. Another option is to use the vacuum forces that arise in the proximity

of dielectrics [38], where a periodic array of pillars with $p = 50\text{nm}$ spacing would correspond to $p = \lambda_{\text{Rb}}/15.6$ for ^{87}Rb atoms ($\lambda_{\text{Rb}} = 780\text{nm}$). Finally, deep subwavelength lattices can be achieved using adiabatic potentials [39] or dynamic modulation of optical lattices [40].

Another possibility for experimental realization is the use of atom-like systems such as color defects in diamond, where techniques for sub-wavelength positioning and coherent manipulation of highly homogenous emitters were recently demonstrated [41–44]. Due to the robustness of topological lattices, inhomogeneous broadening present in such solid-state systems will not significantly change the results as long as the broadening is small compared to the topological energy gap. The creation of subwavelength emitter lattices may also be enabled by the recent progress in the fabrication [45, 46] and patterning [47–49] of monolayer semiconductors, such as transition metal dichalcogenides. Large splitting of the σ_+ , σ_- valley polarizations due to interaction-induced paramagnetic responses was recently demonstrated [50]. Finally, we note that the requirement for deeply subwavelength lattices could potentially be relaxed by integrating the atoms with photonic crystal waveguides as proposed in Ref. [38]. Here, the strong atom-atom interaction mediated by the guided modes of the photonic crystal could give rise to large topological band gaps even when the atoms are spaced $p \approx \lambda/2$ apart.

In summary, we have shown that two-dimensional atomic lattices can be used to create robust quantum optical systems featuring band gaps between photonic bands with non-trivial Chern numbers. For a finite lattice, unidirectional reflection-free edges states form on the system boundaries at energies inside the band gap. These edge modes are robust against imperfections in the lattice as well as scattering and emission into free space. These can be used, e.g. to control emission of individual atoms. A distinguishing feature of the present approach is the intrinsic, built-in nonlinearity associated with quantum emitters in the lattice, which allows one to directly implement and explore strongly interacting topological optical systems. While individual emitters coupled to edge excitations as in Fig. 4 could be directly used for robust implementation of single photon switches and transistors [51, 52], harnessing such interactions could also open up exciting possibilities for studying topological phenomena with strongly interacting photons, including quantum optical analogues of fractional Quantum Hall states. These include exotic states, such as those with filling fractions $\nu = 5/2$ and $\nu = 12/5$, which may feature non-Abelian excitations [7]. In addition, the inherent protection against losses may also be used for the realization of robust quantum nonlinear optical devices for potential applications in quantum information processing and quantum state transfer.

We thank D. Wild, E. Shahmoon, A. High, T. Andersen, N. Yao, J. Taylor, S. Choi, A. Keesling, R. Evans, A.

Sipahigil, P. Kómar and M. Kanász-Nagy for illuminating discussions. We acknowledge funding from the MIT-Harvard CUA, NSF, AFOSR and MURI. JP acknowledges support from the Hungary Initiative Foundation. JB acknowledges funding from the Carlsberg Foundation. DEC acknowledges support from the MINECO “Severo Ochoa” Program (SEV-2015-0522), Fundacio Privada Cellex, CERCA Programme / Generalitat de Catalunya, and ERC Starting Grant FOQAL. Work at Innsbruck is supported by SFB FOQUS of the Austrian Science Fund, and ERC Synergy Grant UQUAM.

-
- [1] K. V. Klitzing, G. Dorda, and M. Pepper, *Physical Review Letters* **45**, 494 (1980).
 - [2] D. C. Tsui, H. L. Stormer, and A. C. Gossard, *Physical Review Letters* **48**, 1559 (1982).
 - [3] M. König, S. Wiedmann, C. Brune, A. Roth, H. Buhmann, L. W. Molenkamp, X.-L. Qi, and S.-C. Zhang, *Science* **318**, 766 (2007).
 - [4] B. I. Halperin, *Physical Review B* **25**, 2185 (1982).
 - [5] R. B. Laughlin, *Physical Review B* **23**, 5632 (1981).
 - [6] A. Kitaev, *Annals of Physics* **303**, 2 (2003).
 - [7] C. Nayak, S. H. Simon, A. Stern, M. Freedman, and S. Das Sarma, *Reviews of Modern Physics* **80**, 1083 (2008).
 - [8] F. D. M. Haldane and S. Raghu, *Physical Review Letters* **100**, 013904 (2008).
 - [9] S. Raghu and F. D. M. Haldane, *Physical Review A* **78**, 033834 (2008).
 - [10] Z. Wang, Y. D. Chong, J. D. Joannopoulos, and M. Soljačić, *Physical Review Letters* **100**, 013905 (2008).
 - [11] K. Liu, L. Shen, and S. He, *Optics Letters* **37**, 4110 (2012).
 - [12] Z. Wang, Y. Chong, J. D. Joannopoulos, and M. Soljačić, *Nature* **461**, 772 (2009).
 - [13] M. C. Rechtsman, J. M. Zeuner, Y. Plotnik, Y. Lumer, D. Podolsky, F. Dreisow, S. Nolte, M. Segev, and A. Szameit, *Nature* **496**, 196 (2013).
 - [14] M. Hafezi, E. A. Demler, M. D. Lukin, and J. M. Taylor, *Nature Physics* **7**, 907 (2011).
 - [15] M. Hafezi, S. Mittal, J. Fan, A. Migdall, and J. M. Taylor, *Nature Photonics* **7**, 1001 (2013).
 - [16] K. Fang, Z. Yu, and S. Fan, *Nature Photonics* **6**, 782 (2012).
 - [17] T. Karzig, C.-E. Bardyn, N. H. Lindner, and G. Refael, *Physical Review X* **5**, 031001 (2015).
 - [18] E. Shahmoon, D. S. Wild, M. D. Lukin, and S. F. Yelin, *Physical Review Letters* **118**, 113601 (2017).
 - [19] A. Asenjo-Garcia, M. Moreno-Cardoner, A. Albrecht, H. J. Kimble, and D. E. Chang, (2017), arXiv:1703.03382.
 - [20] For simplicity we assume that the $|z\rangle$ state is far detuned from resonance, e.g. due to Stark shift. However, one can include the $|z\rangle$ state without detuning as long as there are no polarization-mixing perturbations in the system, as radiation from the $|\sigma_+\rangle$ and $|\sigma_-\rangle$ states is completely decoupled from the transition to the $|z\rangle$ state.
 - [21] N. Y. Yao, C. R. Laumann, A. V. Gorshkov, S. D. Bennett, E. Demler, P. Zoller, and M. D. Lukin, *Physical Review Letters* **109**, 266804 (2012).
 - [22] D. Peter, N. Y. Yao, N. Lang, S. D. Huber, M. D. Lukin,

- and H. P. Büchler, *Physical Review A* **91**, 053617 (2015).
- [23] S. V. Syzranov, M. L. Wall, B. Zhu, V. Gurarie, and A. M. Rey, *Nature Communications* **7**, 13543 (2016).
- [24] C. W. Gardiner and P. Zoller, *Quantum noise: a handbook of Markovian and non-Markovian quantum stochastic methods with applications to quantum optics* (Springer, 2010).
- [25] J. Perczel et al., in preparation (2017).
- [26] M. Antezza and Y. Castin, *Physical Review Letters* **103**, 123903 (2009).
- [27] T. Bienaimé, N. Piovella, and R. Kaiser, *Physical Review Letters* **108**, 123602 (2012).
- [28] W. Guerin, M. O. Araújo, and R. Kaiser, *Physical Review Letters* **116**, 083601 (2016).
- [29] See the Supplemental Material for further discussion.
- [30] C. Bena and G. Montambaux, *New Journal of Physics* **11**, 095003 (2009).
- [31] T. Fukui, Y. Hatsugai, and H. Suzuki, *Journal of the Physical Society of Japan* **74**, 1674 (2005).
- [32] B. A. Bernevig and T. L. Hughes, *Topological Insulators and Topological Superconductors* (Princeton University Press., 2013).
- [33] Y. Plotnik, M. C. Rechtsman, D. Song, M. Heinrich, J. M. Zeuner, S. Nolte, Y. Lumer, N. Malkova, J. Xu, A. Szameit, Z. Chen, and M. Segev, *Nature Materials* **13**, 57 (2013).
- [34] R. Mitsch, C. Sayrin, B. Albrecht, P. Schneeweiss, and A. Rauschenbeutel, *Nature Communications* **5**, 5713 (2014).
- [35] S. John and J. Wang, *Physical Review Letters* **64**, 2418 (1990).
- [36] J. S. Douglas, H. Habibian, C.-L. Hung, A. V. Gorshkov, H. J. Kimble, and D. E. Chang, *Nature Photonics* **9**, 326 (2015).
- [37] B. Olmos, D. Yu, Y. Singh, F. Schreck, K. Bongs, and I. Lesanovsky, *Physical Review Letters* **110**, 143602 (2013).
- [38] A. González-Tudela, C.-L. Hung, D. E. Chang, J. I. Cirac, and H. J. Kimble, *Nature Photonics* **9**, 320 (2015).
- [39] W. Yi, A. J. Daley, G. Pupillo, and P. Zoller, *New Journal of Physics* **10**, 073015 (2008).
- [40] S. Nascimbene, N. Goldman, N. R. Cooper, and J. Dalibard, *Physical Review Letters* **115**, 140401 (2015).
- [41] F. Dolde, I. Jakobi, B. Naydenov, N. Zhao, S. Pezzagna, C. Trautmann, J. Meijer, P. Neumann, F. Jelezko, and J. Wrachtrup, *Nature Physics* **9**, 139 (2013).
- [42] S. Kolkowitz, A. Safira, A. A. High, R. C. Devlin, S. Choi, Q. P. Unterreithmeier, D. Patterson, A. S. Zibrov, V. E. Manucharyan, H. Park, and M. D. Lukin, *Science* **347**, 1129 (2015).
- [43] A. Sipahigil, R. E. Evans, D. D. Sukachev, M. J. Burek, J. Borregaard, M. K. Bhaskar, C. T. Nguyen, J. L. Pacheco, H. A. Atikian, C. Meuwly, R. M. Camacho, F. Jelezko, E. Bielejec, H. Park, M. Lončar, and M. D. Lukin, *Science* **354**, 847 (2016).
- [44] T. Iwasaki, F. Ishibashi, Y. Miyamoto, Y. Doi, S. Kobayashi, T. Miyazaki, K. Tahara, K. D. Jahnke, L. J. Rogers, B. Naydenov, F. Jelezko, S. Yamasaki, S. Nagamachi, T. Inubushi, N. Mizuochi, and M. Hatano, *Scientific Reports* **5**, 12882 (2015).
- [45] Q. H. Wang, K. Kalantar-Zadeh, A. Kis, J. N. Coleman, and M. S. Strano, *Nature Nanotechnology* **7**, 699 (2012).
- [46] C. Robert, D. Lagarde, F. Cadiz, G. Wang, B. Lassagne, T. Amand, A. Balocchi, P. Renucci, S. Tongay, B. Urbaszek, and X. Marie, *Physical Review B* **93**, 205423 (2016).
- [47] H. Li, A. W. Contryman, X. Qian, S. M. Ardakani, Y. Gong, X. Wang, J. M. Weisse, C. H. Lee, J. Zhao, P. M. Ajayan, J. Li, H. C. Manoharan, and X. Zheng, *Nature Communications* **6**, 7381 (2015).
- [48] C. Palacios-Berraquero, D. M. Kara, A. R. P. Montblanch, M. Barbone, P. Latawiec, D. Yoon, A. K. Ott, M. Loncar, A. C. Ferrari, and M. Atature, (2016), arXiv:1609.04244.
- [49] Y. Lin, X. Ling, L. Yu, S. Huang, A. L. Hsu, Y.-H. Lee, J. Kong, M. S. Dresselhaus, and T. Palacios, *Nano Letters* **14**, 5569 (2014).
- [50] P. Back, M. Sidler, O. Cotlet, A. Srivastava, N. Takekura, M. Kroner, and A. Imamoglu, (2017), arXiv:1701.01964.
- [51] B. Dayan, a. S. Parkins, T. Aoki, E. P. Ostby, K. J. Vahala, and H. J. Kimble, *Science* **319**, 1062 (2008).
- [52] W. Chen, K. M. Beck, R. Bucker, M. Gullans, M. D. Lukin, H. Tanji-Suzuki, and V. Vuletic, *Science* **341**, 768 (2013).

Supplemental Material: Topological Quantum Optics in Two-Dimensional Atomic Arrays

The Supplemental Material is organized as follows. In sections 1 and 2 we discuss the theory behind our calculations for the atomic lattice. In section 3 we discuss edge modes on the zig-zag boundary. In section 4 we discuss the influence of lattice size on the decay rate of sub-radiant edge modes. In section 5 we discuss atom-photon bound modes in the bulk of the lattice. Finally, in section 6 we discuss the effects of atomic fluctuations on the spectrum.

1. Dyadic Green's function in free space

The dyadic Green's function $G_{\alpha\beta}(\mathbf{r})$ in Eq. (1) of the Main Text is the solution of the dyadic equation [S1]

$$\frac{\omega^2}{c^2} G_{\nu\beta}(\mathbf{r}) - (\partial_\alpha \partial_\nu - \delta_{\alpha\nu} \partial_\eta \partial_\eta) G_{\alpha\beta}(\mathbf{r}) = \delta_{\nu\beta} \delta(\mathbf{r}). \quad (\text{S1})$$

The components of the Green's function are given by [S1, S2]

$$G_{\alpha\beta}(\mathbf{r}) = -\frac{e^{ikr}}{4\pi r} \left[\left(1 + \frac{i}{kr} - \frac{1}{(kr)^2} \right) \delta_{\alpha\beta} + \left(-1 - \frac{3i}{kr} + \frac{3}{(kr)^2} \right) \frac{x_\alpha x_\beta}{r^2} \right] + \frac{\delta_{\alpha\beta} \delta^{(3)}(\mathbf{r})}{3k^2}, \quad (\text{S2})$$

where $k = \omega/c$ and $\alpha, \beta = x, y, z$ and $r = \sqrt{x^2 + y^2 + z^2}$.

2. Band structure calculation

The modes of the periodic lattice with Bloch quasi-momentum \mathbf{k}_B can be obtained from the eigenvalues and eigenvectors of the complex matrix $E(\mathbf{k}_B)$, which is calculated by substituting Eqs. (1) and (2) from the Main Text into $H|\psi\rangle = \hbar E(\mathbf{k}_B)|\psi\rangle$. Assuming $B = 0$ for simplicity, we obtain

$$E(\mathbf{k}_B) = \left(\omega_A - i \frac{\Gamma_0}{2} \right) \delta_{\alpha\beta} + \frac{3\pi\Gamma_0 c}{\omega_A} \sum_{\mathbf{R}_n \neq 0} e^{i\mathbf{k}_B \cdot \mathbf{R}_n} (G_{\alpha\beta}(\mathbf{R}_n) + G_{\alpha\beta}(\mathbf{R}_n + \mathbf{b})), \quad (\text{S3})$$

where \mathbf{b} is the basis vector pointing from one site to the other within the unit cell of the non-Bravais honeycomb lattice, which has two sites.

To ensure rapid convergence, it is convenient to perform the summation in momentum space. We use Poisson's summation formula [S3-S5] to obtain

$$\begin{aligned} \sum_{\mathbf{R}_n \neq 0} e^{i\mathbf{k}_B \cdot \mathbf{R}_n} G_{\alpha\beta}(\mathbf{R}_n) &= \sum_{\mathbf{R}} e^{i\mathbf{k}_B \cdot \mathbf{R}} G_{\alpha\beta}(\mathbf{R}_n) - G_{\alpha\beta}(\mathbf{0}) \\ &= \frac{1}{\mathcal{A}} \sum_{\mathbf{G}_m} g_{\alpha\beta}(\mathbf{G}_m - \mathbf{k}_B; 0) - G_{\alpha\beta}(\mathbf{0}), \quad (\text{S4}) \end{aligned}$$

where \mathcal{A} is the area of the periodic unit cell and the summation is performed over the reciprocal lattice vectors $\{\mathbf{G}_n\}$ in the 2D plane, which obey $\mathbf{R}_n \cdot \mathbf{G}_m = 2\pi l$ for integers n, m, l and $g_{\alpha\beta}(\mathbf{q}; z=0)$ stands for the Weyl decomposition of the Green's function in terms of 2D plane waves given by [S5, S6]

$$g_{\alpha,\beta}(\mathbf{q}; 0) = \int \frac{dq_z}{2\pi} \frac{1}{k^2} \frac{k^2 \delta_{\alpha\beta} - q_\alpha q_\beta}{k^2 - q^2 - q_z^2 + i\epsilon}, \quad (\text{S5})$$

where $\mathbf{q} = q_x \hat{x} + q_y \hat{y}$ and we restrict ourselves to $\alpha, \beta = x, y$.

The terms on the right-hand side of (S4) are divergent, but after regularizing both terms, their difference becomes finite. Regularization is performed by inserting a Gaussian momentum cut-off $e^{-a_{\text{ho}}^2(q_x^2 + q_y^2 + q_z^2)}$ into the Fourier decomposition of each term [S3-S5]. Upon substitution, the regularized Weyl decomposition becomes

$$g_{\alpha,\beta}^*(\mathbf{q}; 0) = \int \frac{dq_z}{2\pi} \frac{1}{k^2} \frac{k^2 \delta_{\alpha\beta} - q_\alpha q_\beta}{k^2 - q^2 - q_z^2 + i\epsilon} e^{-a_{\text{ho}}^2(q^2 + q_z^2)}. \quad (\text{S6})$$

This integral can be evaluated in a closed form [S5] and the resulting components are given by

$$\begin{aligned} g_{xx}^*(\mathbf{q}; 0) &= (k^2 - q_x^2) \mathcal{I}(\mathbf{q}), \\ g_{yy}^*(\mathbf{q}; 0) &= (k^2 - q_y^2) \mathcal{I}(\mathbf{q}), \\ g_{xy}^*(\mathbf{q}; 0) &= g_{yx}^*(\mathbf{q}; 0) = -q_x q_y \mathcal{I}(\mathbf{q}), \end{aligned} \quad (\text{S7})$$

where we have defined

$$\mathcal{I}(\mathbf{q}) = \chi(\mathbf{q}) \frac{\pi}{\Lambda(\mathbf{q})} [-i + \text{erfi}(a_{\text{ho}} \Lambda(\mathbf{q}))] \quad (\text{S8})$$

with

$$\chi(\mathbf{q}) = \frac{1}{2\pi k^2} e^{-a_{\text{ho}}^2(q_x^2 + q_y^2 + \Lambda(\mathbf{q})^2)} \quad (\text{S9})$$

and

$$\Lambda(\mathbf{q}) = (k^2 - q_x^2 - q_y^2)^{1/2}, \quad (\text{S10})$$

where $\text{Im}(\Lambda) \geq 0$ and $\text{Re}(\Lambda) \geq 0$ is assumed and $\text{erfi}(x)$ stands for the imaginary error function. The regularized Green's function at the source takes the form [S3]

$$G_{\alpha\beta}^*(\mathbf{0}) = \frac{k}{6\pi} \left[\left(\frac{\text{erfi}(ka_{\text{ho}}) - i}{e^{(ka_{\text{ho}})^2}} \right) - \frac{(-1/2) + 2(ka_{\text{ho}})^2}{2\pi^{1/2}(ka_{\text{ho}})^3} \right] \delta_{\alpha\beta}. \quad (\text{S11})$$

It can be shown using the methods developed in [S3] that $\exp(k^2 a_{\text{ho}}^2) [1/\mathcal{A} \sum_{\mathbf{G}_m} g_{\alpha\beta}^*(\mathbf{G}_m - \mathbf{k}_B; 0) - G_{\alpha\beta}^*(\mathbf{0})]$ approaches the value of the left-hand side of Eq. (S4) as the limit $a_{\text{ho}} \rightarrow 0$ is taken [S5]. Therefore, in order to numerically perform the summation in momentum space, it is sufficient to choose a small, but finite a_{ho} such that $a_{\text{ho}} \ll \lambda$.

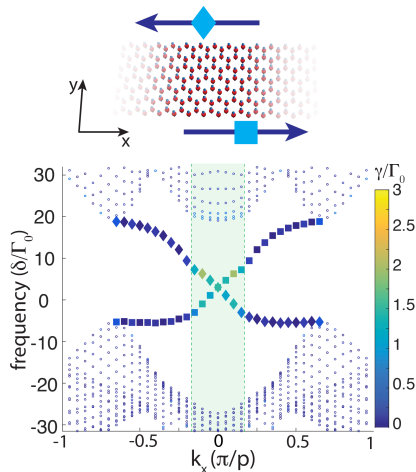


FIG. S1. Edge modes on the zig-zag boundary of a honeycomb lattice. Edge modes in the bottom half of the band gap have quasi-momenta $k_B < \omega/c$ and are short-lived. Modes in the top half of the gap have quasi-momenta $k_B > \omega/c$ and are long-lived. Relevant parameters are $\lambda = 790\text{nm}$, $\Gamma_0 = 6\text{MHz}$ and $p = 0.05\lambda$ and the spectrum was obtained from a lattice with 80×41 atoms with periodic boundary conditions along the longer dimension. States with more than 67% of their total amplitude on the top/bottom four atom rows are classified as edge states.

3. Edge modes on the zig-zag boundary

In addition to the bearded and armchair modes, a honeycomb lattice can also be terminated by a zig-zag boundary. Fig. S1 shows the spectrum of the edge modes on such a boundary. Edge modes in the bottom half of the band gap have quasi-momenta $k_B < \omega/c$ and are short-lived, whereas modes in the top half of the gap have quasi-momenta $k_B > \omega/c$ and are long-lived. By tuning the frequency of a laser to be resonant with the modes in the top half of the gap, we can predominantly excite the long-lived edge modes of the zig-zag edge.

4. Influence of system size on decay rate of bearded edge modes

For an infinite lattice, modes with quasi-momenta $k_B > \omega/c$ are decoupled from free-space modes and, therefore, do not decay. In contrast, for finite lattices even such modes have a finite lifetime. Fig. S2 shows the decay rate of the bearded edge modes with $k_B > \omega/c$ as the total number of atoms in the lattice is varied. The interatomic spacing is assumed to be fixed at $p = \lambda/20$. The decay rate of the modes scales approximately as $\sim 1/\sqrt{N}$, where N is the total number of atoms in the 2D lattice. This scaling is consistent with the observation that, since edge modes are confined to the boundaries, they explore only the 1D perimeter of the lattice, which

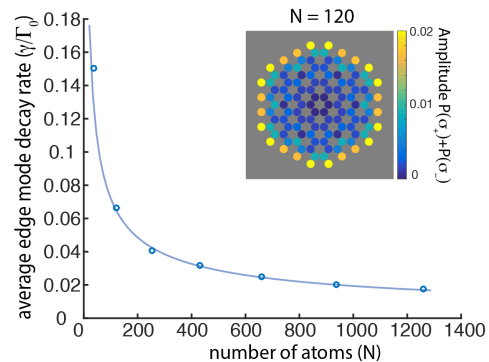


FIG. S2. Scaling of the decay rate of the edge modes on the bearded boundary as a function of the total number of atoms in the hexagonal-shaped atom lattice. The decay rate scales approximately as $\sim 1/\sqrt{N}$. The numerical fit to the data points $\sim 1/N^{0.57}$ is shown as a solid line. To obtain each point in the plot, a hexagonal-shaped lattice of N atoms with bearded boundaries was considered with $p = \lambda/20$. The average decay rate was obtained by averaging the decay rates of all edge states inside the band gap. The inset shows the probability amplitudes of a bearded edge state on a lattice of $N = 120$ atoms.

scales with \sqrt{N} .

5. Bulk excitations within the band gap

Fig. S3 shows the atom-photon bound steady state that forms when an atom in the bulk of the lattice is driven by a laser with its frequency inside the band gap. Due to the off-resonant excitation of the bulk modes, the bound state is confined to the neighborhood of the driven atom. Since the band gap arises from the Zeeman-splitting of the $|\sigma_+\rangle$ and $|\sigma_-\rangle$ levels, the bulk modes above and below the band gap couple more strongly to light polarized along $\hat{\sigma}_+$ and $\hat{\sigma}_-$ respectively. Since the modes close to the center of the Brillouin zone and immediately above the gap are short-lived, a laser with polarization σ_+ excites a shorter lived bound state with $\gamma = \Gamma_0/4.7$, whereas a laser with polarization σ_- yields $\gamma = \Gamma_0/7.7$. For an \hat{x} polarized laser we obtain $\gamma = \Gamma_0/5.7$.

6. Effect of fluctuating atomic positions

The Hamiltonian in Eq. (1) of the Main Text assumes that the position of the atoms is fixed at the sites of the lattice. In practice, even when the atoms are tightly trapped and are occupying their motional ground state, their position will fluctuate around the lattice sites. These quantum fluctuations are uncorrelated between different sites. To quantify how the quantum fluctuations in atomic positions affect our results, we assume a harmonic trapping potential of frequency ω_{ho} , with the

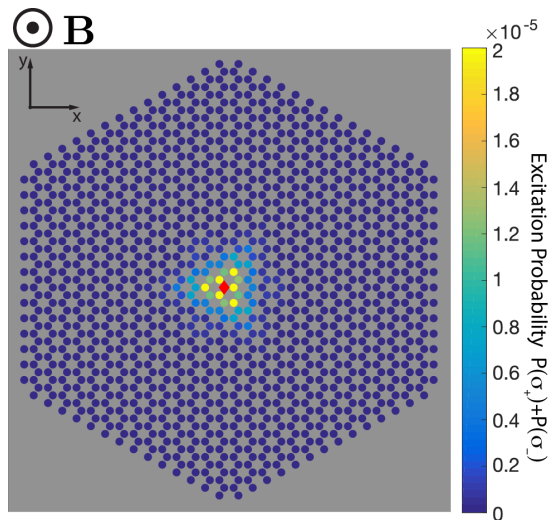


FIG. S3. A sub-radiant atom-photon bound state forms when an atom in the bulk of the lattice (marked with a red diamond) is driven by a laser with its frequency inside the band gap. The decay rate of the bound state is sensitive to the polarization of the driving laser. Relevant parameters are $N = 1260$, $\lambda = 790\text{nm}$, $\Gamma_0 = 6\text{MHz}$ and $p = 0.05\lambda$. The strength of the drive is $\Omega = 1\Gamma_0$ and the frequency of the laser is tuned such that $\omega_L = \omega_A + 10\Gamma_0$. The driving laser is adiabatically switched on with a sigmoid profile $\Omega(t) = \Omega [1 + \exp(-(t - 3\Gamma_0^{-1})/0.3\Gamma_0^{-1})]^{-1}$. The figure shows a snapshot at $t = 10\Gamma_0^{-1}$.

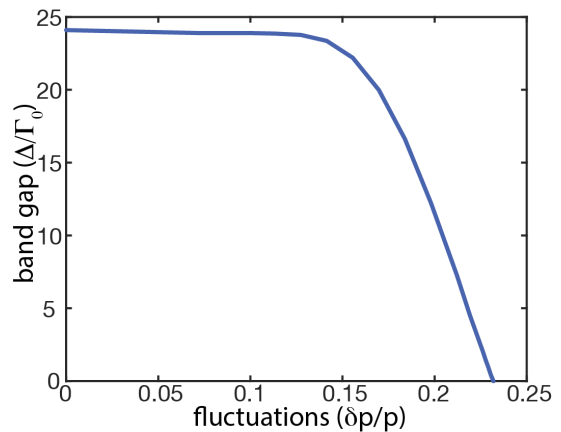


FIG. S4. Size of the maximum gap size Δ_{\max} as the atomic positions fluctuate with amplitude δp around the lattice sites with fixed interatomic spacing $p = 0.05\lambda$. When the amplitude of the fluctuations is less than 15% of the interatomic spacing p , the band structure is not significantly affected.

corresponding spatial extent of the ground state oscillations on the order of $\delta p = \sqrt{\hbar/(2m\omega_{\text{ho}})}$. We then average the dyadic Green's function in the Hamiltonian with respect to the ground state fluctuations [S3, S5]. Fig. S4 shows how the size of the band gap between the topological bands changes as the magnitude of δp is varied as a fraction of the interatomic spacing p . Larger fluctuations smear out the well-defined phase between different atoms and eventually the gap closes. However, when the extent of the fluctuations is less than 15% of the interatomic spacing, the size of the gap (and the band structure as a whole) is not significantly affected. This shows that our results are robust against moderate fluctuations in atomic positions around the lattice sites.

-
- [S1] H. T. Dung, L. Knöll, and D.-G. Welsch, *Physical Review A* **57**, 3931 (1998).
 - [S2] O. Morice, Y. Castin, and J. Dalibard, *Physical Review A* **51**, 3896 (1995).
 - [S3] M. Antezza and Y. Castin, *Physical Review Letters* **103**, 123903 (2009).
 - [S4] M. Antezza and Y. Castin, *Physical Review A* **80**, 013816 (2009).
 - [S5] J. Perczel et al., in preparation (2017).
 - [S6] W. C. Chew, *Wave and fields in inhomogeneous media* (IEEE, 1999).